Adducts of Ferrocenylboranes and Pyridine Bases: Generation of Charge-Transfer Complexes and Reversible Coordination Polymers☆

Marco Fontani[b], Frank Peters[a], Wolfgang Scherer[a], Wolfgang Wachter[a], Matthias Wagner*[a], and Piero Zanello[b]

Anorganisch-chemisches Institut, Technische Universität München[a],
Lichtenbergstraße 4, D-85747 Garching b.München, Germany
Fax: (internat.) + 49(0)89/28913473
E-mail: wagner@arthur.anorg.chemie.tu-muenchen.de

Universitá di Siena, Dipartímento di Chimica[b],
Pian dei Mantellini 44, I-53100 Siena, Italy
Fax: (internat.) + 39-577/280405
E-mail: zanello@unisi.it

Received April 1, 1998

Keywords: Iron / Boron / Ferrocene / Charge-transfer complexes / Coordination polymers

Compared to parent ferrocene, the redox potential of the Fe^{II}/Fe^{III} transition is shifted to much more cathodic values in B–N adducts **1**·Do and **2**·$(Do)_2$ of borylated ferrocenes $FcBMe_2$ (**1**) and 1,1′-fc$(BMe_2)_2$ (**2**) with pyridine bases Do [Fc: $(C_5H_5)Fe(C_5H_4)$; fc: $(C_5H_4)Fe(C_5H_4)$; Do: γ-picoline, 4-(dimethylamino)pyridine, *N*-(*n*-propyl)-4-(4′-pyridyl)pyridinium hexafluorophosphate]. Electron donation by one single BMe_2·Do substituent at the cyclopentadienyl ligand is approximately equal to the positive inductive effect of the five methyl groups in a C_5Me_5 (cp*) moiety. Using the bidentate nitrogen ligand 4,4′-bipyridine (bipy), the dark-purple dimetallic complex **1**·bipy·**1** is obtained upon reaction with 2 equiv. of **1**. **1**·bipy·**1** has been structurally characterized by X-ray crystallography. The compound tolerates loss of two electrons at the ferrocene groups, as well as two one-electron reductions at the bipy linker. Dark purple coloured coordination polymers $[\mathbf{2}\cdot bipy]_n$ are accessible from bipy and 1 equiv. of the diborylated derivative **2**. The intense colours of **1**·bipy·**1** and $[\mathbf{2}\cdot bipy]_n$ are indicative of charge-transfer interactions between the electron-rich ferrocene fragments and the viologen-like R_3B–bipy–BR_3 acceptor. Neat, solid $[\mathbf{2}\cdot bipy]_n$ is thermally stable up to 240 °C, but in the presence of toluene, polymerization is fully reversible at about 85 °C.

Introduction

Multimolecular arrays in which metal complexes are joined by rigid (electroactive) bridges represent a highly promising class of compounds, due to the potential properties of these materials such as electrical conductivity,[1] magnetism[2] and liquid-crystalline behaviour.[3] Two main lines of research that are particularly relevant in the context of this paper, concern: (a) Poly(ferrocenes) **A** derived from strained, ring-tilted *ansa*-ferrocenes by thermal[4][5] or catalytic[6] ring-opening polymerization (Figure 1). (b) Low-dimensional solids **B** comprised of coordinatively unsaturated metal complex fragments and bridging dihapto ligands. Among the latter, 4,4′-bipyridine (bipy) and 1,2-bis(4-pyridyl)ethane (pyetpy) are particularly prominent (**B**, Figure 1).[7]

Figure 1. Poly(ferrocenes) **A** and bipy-bridged coordination polymers **B**

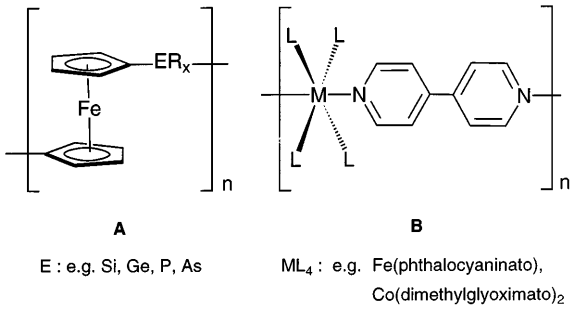

Our group is currently developing a novel synthetic approach to oligonuclear complexes and organometallic polymers, which is based on the facile formation of boron−nitrogen bonds and thus provides a convenient means of connecting mononuclear metal-containing building blocks.[8][9][10][11] This concept appeared to us to be well-suited for the generation of molecular materials combining the advantages of poly(ferrocenes) (e.g. thermal and chemical inertness of the ferrocene backbone; reversible redox processes) and bipy coordination polymers (e.g. facile synthesis; electron-accepting properties of the bipy unit). It will be shown in this paper that, starting from readily available borylated ferrocenes,[12][13][14][15][16] the addition of 4,4′-bipyridine or 1,2-bis(4-pyridyl)ethane gives dimetallic complexes and polymeric materials by B−N adduct formation (Schemes 1 and 2).

A variety of intriguing properties can be expected to result from the combination of ferrocene and pyridine bases, and the following points will be addressed:

(1) The ligand 4,4′-bipyridine has two coordination sites, which may influence each other by the delocalized π-electron system. The question then arises as to what extent

  1434−1948/98/1010−1453 $ 17.50+.50/0

N→B σ bonding at one nitrogen centre lowers the Lewis basicity of the remaining free N atom, i.e. whether the formation of $R_3B{\cdot}bipy{\cdot}BR_3$ involves stable and isolable $R_3B{\cdot}bipy$ intermediates.

(2) Closely related to the aforementioned question is the problem as to whether a bipy spacer allows electronic communication between two pendant ferrocenylborane units (**1**·bipy·**1**; Scheme 1).

Scheme 1

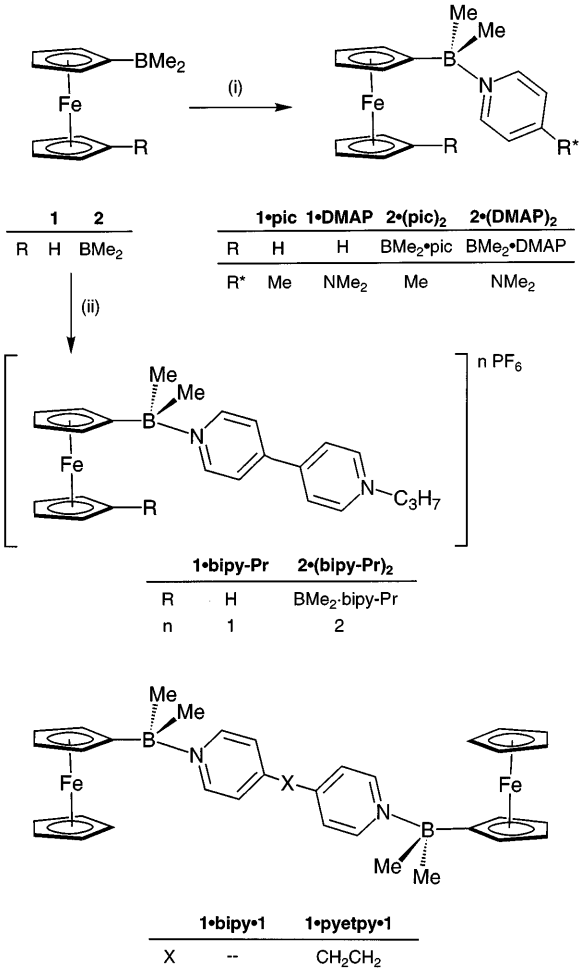

Reagents: (i) **1**·pic/**1**·DMAP: **1** + 1 pic/DMAP; toluene, ambient temp. **2**·$(pic)_2$/**2**·$(DMAP)_2$: **2** + 2 pic/DMAP; toluene, ambient temp. (ii) **1**·bipy-Pr: **1** + 1 bipy-Pr; acetonitrile, ambient temp. **2**·$(bipy\text{-}Pr)_2$: **2** + 2 bipy-Pr; acetonitrile, ambient temp.

Moreover, comparison of the electrochemical data of the Lewis acid/base complexes **1**·pic, **1**·DMAP, **2**·$(pic)_2$ and **2**·$(DMAP)_2$ (Scheme 1), featuring the moderately strong electron donor γ-picoline (pic; pK_a = 6.02; in water, 25°C)[17] on the one hand, and the more basic 4-(dimethylamino)pyridine (DMAP; pK_a = 9.71; in water, 20°C)[18] on the other, will yield information on the influence of tetracoordinate boron substituents on the redox potential of the ferrocene fragment.

(3) 4,4′-Bipyridine-1,1′-diyldiboranes **C** are analogues of the bis-quaternary salts of 4,4′-bipyridine ($\mathbf{D}^{2+}$, "viologens"), which behave as perfectly reversible two-step redox

Figure 2. B−N adducts **C** as structural and electrochemical analogues of the two-step redox system viologen $\mathbf{D}^{2+}$

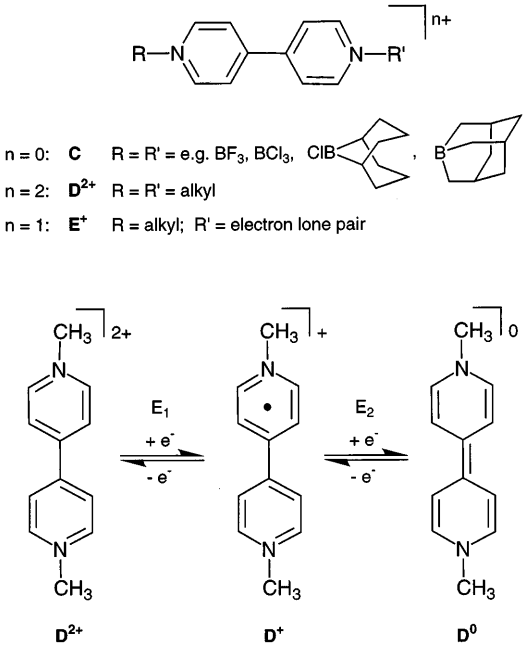

systems in polar aprotic solvents such as acetonitrile and dimethylformamide (Figure 2).[19]

Consequently, derivatives of $\mathbf{D}^{2+}$ have found widespread use as electron acceptors[20][21] and electron carriers,[22] and it is in the latter context that the incorporation of viologens into polymers has been thoroughly investigated.[23][24][25][26] To a large extent, these polymeric materials retain the chemical and electrochemical properties of the monomeric species $\mathbf{D}^{2+}$, although the first reduction (E_1) of polyviologens usually occurs at a more anodic, and the second (E_2) at a more cathodic potential, compared to the corresponding monomers. Thus, in polymeric viologens, the difference ΔE between the two potential values was found to be about twice as large as that in the monomers, and this effect is observable even in oligomers with only 2 or 3 repeating units.[25] This behaviour is indicative of a certain degree of electronic communication between the electroactive sites, which has been attributed to intramolecular interactions among neighbouring pendant viologen cation radicals. Given this background, it will be interesting to see how the electronic behaviour of polymeric viologens changes when the highly flexible backbones used to date are substituted for the more rigid 1,1′-ferrocenediyl spacer [cf. **2**·$(bipy\text{-}Pr)_2$; Scheme 1]. For a general discussion of $L_nM{\cdot}bipy{\cdot}ML_n$ adducts (ML_n: main-group Lewis acid) and the respective radicals formed upon one-electron reduction, the reader is referred to the work of Kaim et al.[27][28][29][30]

(4) The synthesis of aggregates composed of electron-donating ferrocene units and electron-accepting viologen bridges may lead to charge-transfer (CT) processes between the two components. This assumption is based on the observation of pronounced CT interactions between the ferrocene backbone and its pendant 2,2′-bipyridylboronium substituents in the case of related systems **F** (Figure 3).[31][32]

Figure 3. View of the charge-transfer complex **F**

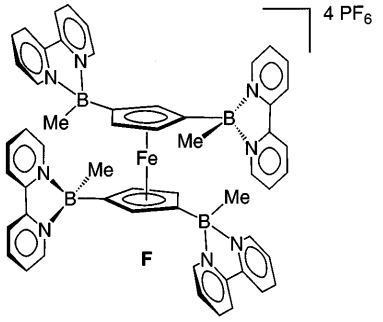

Results and Discussion

In the following, the numbers **1** and **2** are used to denote derivatives of mono- and diborylated ferrocenes, respectively. These numbers are followed by a specification of the coordinating pyridine, i.e. pic, DMAP, bipy, pyetpy and bipy-Pr [*N*-(*n*-propyl)-4-(4′-pyridyl)pyridinium hexafluorophosphate[26]]. The term "Do" stands for all these cited pyridine donors in general.

Synthesis

1·pic, **1**·DMAP and **2**·$(pic)_2$, **2**·$(DMAP)_2$ were prepared by mixing toluene solutions of the appropriate nitrogen base and **1** (molar ratio 1:1) or **2** (molar ratio 2:1) at ambient temperature (Scheme 1). Orange crystalline solids were obtained in almost quantitative yields. Even in solution, the compounds show only moderate sensitivity towards moisture, but **2**·$(pic)_2$ and **2**·$(DMAP)_2$ are rapidly oxidized on exposure to air (see below). The syntheses of the ionic adducts **1**·bipy-Pr and **2**·$(bipy\text{-}Pr)_2$ were performed in acetonitrile (Scheme 1). From the dark, purple-red reaction mixtures, the compounds were isolated as almost black crystals. The dinuclear complex **1**·bipy·**1**, which was obtained from toluene solutions of **1** and bipy (molar ratio 2:1), also forms dark-purple crystals and gives intensely red-coloured solutions in toluene as well as in chloroform. In contrast, the related compound **1**·pyetpy·**1** is orange, both in solution and in the solid state, and thus resembles the pic and DMAP adducts described above.

While alkyl bipyridinium systems $\mathbf{E}^+$ (R = alkyl; R′ = electron lone pair; n = 1) are readily accessible (Figure 2),[26] we have not been able to isolate a stable 1:1 adduct of bipy with **1**, even though this species is likely to be abundant in an equimolar solution of the two components. Communication of both nitrogen termini in bipy seems to be observable only when electrophiles of very high Lewis acidity are used for nitrogen coordination, and this condition is apparently not met with **1**.

When diborylated ferrocene **2** in $CHCl_3$ is layered with one equiv. of bipy in CH_2Cl_2, polymeric [**2**·bipy]$_n$ is obtained as a purple microcrystalline solid, which is insoluble in all common non-coordinating solvents. In an attempt to grow single crystals suitable for X-ray crystallography, we tried to slow down the reaction rate by replacing the highly Lewis acidic **2** with its corresponding picoline adduct **2**·$(pic)_2$ (Scheme 2). Using this method, black rhombic crystals of [**2**·bipy]$_n$ grew within 24 h, and it was shown that coordinated pic may be substituted for bipy, even though the former is a much stronger base [pic: pK_a = 6.02;[17] bipy: pK_a(1) = 4.82, pK_a(2) = 3.17;[33] in water, 25°C]. A driving force for this reaction clearly lies in the precipitation of [**2**·bipy]$_n$, which is thus continuously removed from the reaction mixture, thereby shifting the equilibrium towards polymer formation. Polymerization can be reversed by treating purple [**2**·bipy]$_n$ with excess picoline. From the resulting orange solutions, uncomplexed bipy and **2**·$(pic)_2$ can be recovered quantitatively. A polymeric product is also obtained from **2** or **2**·$(pic)_2$ upon reaction with one equiv. of 1,2-bis(4-pyridyl)ethane (pyetpy). Like the dinuclear species **1**·pyetpy·**1**, and unlike **1**·bipy·**1** and [**2**·bipy]$_n$, [**2**·pyetpy]$_n$ exhibits the orange colour usually observed for ferrocenes bearing tetracoordinate boron substituents.

Scheme 2. Preparation of the coordination polymers [**2**·bipy]$_n$ and [**2**·pyetpy]$_n$

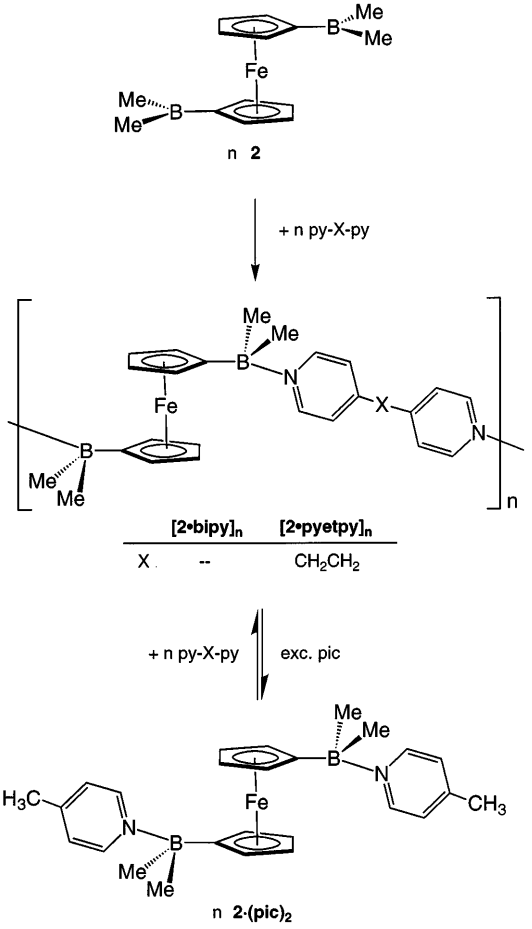

NMR Spectroscopy

It is a characteristic feature of B−N donor−acceptor compounds that a dynamic equilibrium exists in solution involving the four-coordinate species and the respective free acids and bases. The chemical shifts observed in the NMR spectra are thus a weighted average between those of the adducts and those of the uncomplexed components. Obviously, the relative amount of an adduct increases when the

solution becomes more concentrated. Therefore, we have used saturated solutions for all NMR spectroscopic measurements to ensure full reproducibility of the data and to obtain chemical shift values as close as possible to the resonances of **1**·Do and **2**·$(Do)_2$. Since the B−N adducts under investigation possess different solubilities in the chosen solvents ($CDCl_3$, CD_3CN), a quantitative comparison, particularly of their ^{11}B-NMR data, is problematic. We have therefore restricted the discussion of NMR spectra to a qualitative level.

Compared to the ^{11}B-NMR spectra of **1** [$\delta(^{11}B) = 70.5$] and **2** [$\delta(^{11}B) = 72.1$], the resonances of **1**·Do and **2**·$(Do)_2$ show large upfield shifts upon addition of the pyridine bases [$\delta(^{11}B) = -3.0$ to 15.0], giving good evidence for B−N adduct structures with four-coordinate boron centres.[34] The relative base strengths of the different pyridines are nicely reflected in the ^{11}B chemical shift values of the B−N complexes, with stronger donors leading to a better shielding of the boron centre: $\delta(^{11}B) = -3.0$ (**1**·DMAP), 0.4 (**1**·pic), 7.5 (**1**·bipy-Pr); 6.2 (**1**·pyetpy·**1**), 15.1 (**1**·bipy·**1**). A similar correlation holds for the adducts of diborylated **2**, but the ^{11}B-NMR signals of the diadducts generally appear at lower field compared to those of the corresponding monoadducts, e.g. $\delta(^{11}B) = 0.4$ (**1**·pic), 15.0 [**2**·$(pic)_2$]. When a large excess (0.5 ml) of pic is added to a solution of **2**·$(pic)_2$ in $CDCl_3$, the boron resonance closely approaches that of **1**·pic [**2**·$(pic)_2$ and excess of pic: $\delta(^{11}B) = 0.0$]. This finding is in good agreement with the assumption of a dissociation equilibrium, which is shifted towards adduct formation in the presence of free base. To gain a deeper insight into this phenomenon, we have investigated the dynamic behaviour of equimolar mixtures of **2** with pic and DMAP in [D_8]toluene at various temperatures by ^{11}B-NMR spectroscopy. In the case of pic, only one extremely broad resonance is detected at ambient temperature [$\delta(^{11}B) \approx 33$]. Upon warming, the signal sharpens considerably, but no significant change of its chemical shift is observed [+60°C: $\delta(^{11}B) = 35.0$; $h_{1/2} = 720$ Hz]. The signal vanishes upon cooling to +15°C. At −10°C, two very broad humps become visible at $\delta(^{11}B) = 70$ and 0, while at −50°C the resonances appear at $\delta(^{11}B) = 73.6$ ($h_{1/2} = 1780$ Hz) and −0.6 ($h_{1/2} = 720$ Hz). In the DMAP case, two ^{11}B-NMR signals are observed even at ambient temperature [$\delta(^{11}B) = 71.0$ ($h_{1/2} = 320$ Hz), −2.8 ($h_{1/2} = 640$ Hz)]. Coalescence of these signals occurs in the temperature range between +80 and +90°C, and at +110°C only one resonance is seen at $\delta(^{11}B) = 35$ ($h_{1/2} = 1360$ Hz). These data suggest that at ambient temperature, and when the N donor is of moderate basicity (pic), the base rapidly fluctuates between the two boron atoms of **2**. The observed ^{11}B-chemical shift is thus time-averaged. In contrast, the stronger donor DMAP comes to a rest at one of the BMe_2 centres under these conditions, and the ^{11}B-NMR spectrum is indicative of the presence of one tri- and one tetracoordinate boron atom. The free activation enthalpies $\Delta G^{\neq}$ of the dynamic processes can be estimated as 45 ± 2 kJ mol^{-1} (pic) and 58 ± 2 kJ mol^{-1} {DMAP; $\Delta G^{\neq} = 19.14\ T_c\ [10.32 + \log(T_c k_c^{-1}]$; $k_c = 2.22 \cdot \Delta\nu$}[35].

In the ^{1}H- and ^{13}C-NMR spectra, one observes only minor changes of the chemical shifts of the pyridine bases upon B−N adduct formation. This finding is in contrast to what was expected, since in the case of e.g. compounds **C**, a pronounced dependence of the bipy proton ^{1}H signals on the nature of the coordinated borane has been reported, e.g. R, R′ = BF_3: $\delta(^1H) = 8.63, 9.54$; R, R′ = 1-boraadamantane: $\delta(^1H) = 8.31, 8.84$ ([D_6]DMSO).[36] For most derivatives of **C**, these values are intermediate between those of free bipy [$\delta(^1H) = 7.79, 8.63$] and those of the bis-quaternary $\mathbf{D}^{2+}$ [R, R′ = CH_3: $\delta(^1H) = 8.68, 9.21$].[36] It has thus been argued that coordination of a highly Lewis acidic borane is mirrored by a pronounced deshielding of the bipy protons in the ^{1}H-NMR spectrum.[36] Even though this correlation may serve as a useful rule of thumb, a quantitative interpretation requires more detailed scrutiny, and other factors, such as magnetic anisotropy effects, also have to be taken into account. For example, the reasons why the bipy protons in the BF_3 adduct experience a large downfield shift, even though BF_3 is a rather weak electrophile,[37][38] still remain obscure.

The ^{1}H-NMR resonances of the $FcBMe_2$ moiety are more informative, showing characteristic upfield shifts upon treatment with pyridine bases: (a) The signal of the BMe_2 fragment, which appears at $\delta(^1H) = 0.82$ in uncomplexed **1**, is found in the corresponding B−N adducts at $\delta(^1H) = 0.30$ (**1**·bipy-Pr), 0.27 (**1**·pic), 0.16 (**1**·DMAP) and at $\delta(^1H) = 0.40$ (**1**·bipy·**1**), 0.29 (**1**·pyetpy·**1**). (b) The protons of the C_5H_4 ring bearing the boryl substituent resonate at $\delta(^1H) = 4.37, 4.59$ in the case of **1**, but are significantly more shielded in **1**·bipy-Pr [$\delta(^1H) = 4.08, 4.19$], **1**·pic [$\delta(^1H) = 4.03, 4.16$], **1**·DMAP [δ⊥ft parenthesis^{1}H) = 3.97, 4.09] and in **1**·bipy·**1** [$\delta(^1H) = 4.13, 4.27$] and **1**·pyetpy·**1** [$\delta(^1H) = 4.04, 4.18$]. These data clearly indicate that not only the ^{11}B-NMR spectra, but also the cited proton shifts can be taken as a measure of the pK_a values of the coordinating pyridines. Similar effects as described for **1** are operative in the case of diborylated derivatives, cf. **2**: $\delta(^1H) = 0.84$ (BCH_3), 4.31, 4.44 (C_5H_4); **2**·$(pic)_2$: $\delta(^1H) = 0.34$ (BCH_3), 3.99, 4.13 (C_5H_4).

The ^{13}C-NMR data of **1**, **2** on the one hand, and of **1**·Do, **2**·$(Do)_2$ on the other, show similar changes and therefore do not merit further discussion.

Infrared Spectroscopy

The infrared spectrum of a pyridine base is modified when the non-bonding pair of electrons on the nitrogen atom is donated into a vacant orbital of an electron acceptor. Consequently, a comparison of the IR data (KBr disc) of **1**, **2** and of the free donors Do with **1**·Do and **2**·$(Do)_2$ reveals a number of alterations characteristic of B−N adduct formation, which will be described here in detail for the oligometallic complexes **1**·bipy·**1** and [**2**·bipy]$_n$ only (Table 1).

B−N Vibration: The values of the B−N stretching modes are of particular importance in obtaining information about the stability of the Lewis acid/base pairs under investigation. The B−N frequencies of solid (KBr disc)

BCl_3·pyridine and BF_3·pyridine have been reported to occur at $\tilde{\nu}$ = 1113 cm^{-1}[39] and $\tilde{\nu}$ = 1112 cm^{-1}[40], respectively. For a series of complexes BX_3·pyridine (X: H, F, Cl, Br) in $CHCl_3$ solution, the corresponding bands are found in the 1102−1090 cm^{-1} interval. They are shifted to lower values when pyridines bearing electron-withdrawing substituents at the 4-position are used (e.g. BCl_3·4-chloropyridine: 1076 cm^{-1}).[41]

Table 1. Infrared bands [cm^{-1}] of selected compounds **1**·Do and **2**·$(Do)_2$ (KBr disc) in the characteristic regions 1650−1450 cm^{-1} (C=C and C=N stretch) and 1100−1050 cm^{-1} (B−N vibration)

1·pic	**1**·DMAP	**2**·$(pic)_2$	**2**·$(DMAP)_2$	**1**·bipy·**1**	[**2**·bipy]$_n$
1628	1636	1628	1638	1622	1622
−	1544	−	1552	1540	1540
1507	−	1508	−	1493	1493
1104	1104	−	−	1100	−
1068	1076	1066	1077	1075	1075
1058	1058	1047	1060	1058	1061

1·pic	**1**·DMAP	**2**·$(pic)_2$	**2**·$(DMAP)_2$	**1**·bipy·**1**	[**2**·bipy]$_n$
1606	1603			1590	1645
1563	1537			1531	1569
1497	1519			1487	1509

[a] *N,N′*-Bis(*n*-propyl)-4,4′-bipyridinium hexafluorophosphate.

1·bipy·**1** exhibits three bands in the region of interest ($\tilde{\nu}$ = 1100 cm^{-1}, 1075 cm^{-1}, 1058 cm^{-1}), while [**2**·bipy]$_n$ shows only two such absorptions at $\tilde{\nu}$ = 1075 cm^{-1} and 1061 cm^{-1} (Table 1). It can thus be concluded that the band at $\tilde{\nu}$ = 1100 cm^{-1} is probably not caused by a B−N vibration. The band at $\tilde{\nu}$ = 1075 cm^{-1} appears not only in **1**·bipy·**1** and [**2**·bipy]$_n$, but also in the IR spectra of the free Lewis acids **1** and **2**. Moreover, it does not show the isotope doublet structure ($^{10}B/^{11}B$) that would be expected for a vibration involving the motion of a boron atom. Given this background, the band at $\tilde{\nu}$ = 1058 cm^{-1} (1061 cm^{-1}) is tentatively assigned to the B−N stretching mode of **1**·bipy·**1** ([**2**·bipy]$_n$). It has to be concluded that the B−N bonds in **1**·Do and **2**·$(Do)_2$ are not very strong, which is in accord with the thermal behaviour of these compounds in solution, as well as with the NMR spectroscopic results outlined above.

C=C/C=N Vibration: The region between $\tilde{\nu}$ = 1650 cm^{-1} and $\tilde{\nu}$ = 1450 cm^{-1}, showing three bands at 1622 cm^{-1}, 1540 cm^{-1} and 1493 cm^{-1} both for **1**·bipy·**1**, and for [**2**·bipy]$_n$, also merits further discussion (Table 1). Neither **1** nor **2** exhibits significant absorptions in this region of the spectrum, and thus we may safely assume that these bands are due to C=N and C=C stretching modes of the bipy fragments. Compared to the free base, which shows bands at $\tilde{\nu}$ = 1590 cm^{-1}, 1531 cm^{-1} and 1487 cm^{-1} (KBr disc), the adduct absorptions are shifted by 32 cm^{-1}, 9 cm^{-1} and 6 cm^{-1} towards higher wavenumbers. Similar changes have previously been reported for other complexes of pyridines with main-group Lewis acids.[39][41] The pronounced shift of the highest energy band may therefore be used as a valuable diagnostic tool to investigate (a) the degree of **1**·bipy·**1** dissociation in solution on a very fast time scale, and (b) the molecular structure of solid [**2**·bipy]$_n$.

(a) All infrared frequencies exhibited by solid **1**·bipy·**1** (KBr disc) are also found in CH_2Cl_2 solution. The solution spectrum, however, reveals two additional weak bands ($\tilde{\nu}$ = 1597 cm^{-1}, 1517 cm^{-1}) in the characteristic region between $\tilde{\nu}$ = 1650 cm^{-1} and 1450 cm^{-1}, thereby indicating the presence of a second species that is not found in the solid state. Since the additional absorptions do not match those of free bipy in CH_2Cl_2 ($\tilde{\nu}$ = 1592 cm^{-1}, 1535 cm^{-1}, 1485 cm^{-1}), they are most likely caused by the monoadduct **1**·bipy. This molecule may be formed in a dynamic equilibrium by the dissociation of a small proportion of **1**·bipy·**1**, as has already been suggested from an inspection of the ^{11}B-NMR spectra.

(b) An intense band at $\tilde{\nu}$ = 1622 cm^{-1} and the absence of an absorption at $\tilde{\nu}$ = 1590 cm^{-1} in the infrared spectrum of [**2**·bipy]$_n$ provides strong evidence in favour of the proposed adduct structure. The amount of any free bipy that might have co-crystallized with [**2**·bipy]$_n$ is beyond the detection limit of the IR spectrometer. The question then remains as to whether [**2**·bipy]$_n$ consists mainly of short oligomeric fragments, or whether it is a well-organized coordination polymer. One way of distinguishing between these two structural motifs is to evaluate the amount of uncomplexed BMe_2 substituents or of terminal bipy units with one coordinating and one uncomplexed nitrogen atom. The two types of chain end should be equally abundant in [**2**·bipy]$_n$, but we will focus our attention on the latter, which is easier to detect by IR spectroscopy. Terminal bipy ligands have a less symmetrical environment than bridging bipy, which leads to the appearance of additional infrared lines. For example, monosubstituted [bipy-Pr]PF_6 exhibits (among others) four well-resolved C=C/C=N stretching frequencies at $\tilde{\nu}$ = 1597 cm^{-1}, 1548 cm^{-1}, 1526 cm^{-1} and 1496 cm^{-1}, whereas the bis-quaternary salt [Pr−bipy−Pr]$(PF_6)_2$ shows only two lines in this spectral range with intermediate values of $\tilde{\nu}$ = 1569 cm^{-1} and 1509 cm^{-1}. In the characteristic region, the frequency pattern of [**2**·bipy]$_n$ closely resembles that of [Pr−bipy−Pr]$(PF_6)_2$ and is absolutely identical with the IR spectrum of **1**·bipy·**1**. These findings suggest that there are far less terminal than internal bipy ligands present in [**2**·bipy]$_n$ and are thus consistent with the proposed polymeric structure. It should be noted, however, that on the basis of the infrared data discussed, the presence of cyclic structures *cyclo*-[**2**·bipy]$_n$ cannot be ruled out.

Solid-State Structure of 1·bipy·1

Dark-purple crystals of **1**·bipy·**1** (Figure 4, Table 2) were grown from toluene/hexane (1:1) in the triclinic space group *P*$\bar{1}$ with two crystallographically independent molecules in the asymmetric unit (**1**·bipy·$\mathbf{1}_A$, **1**·bipy·$\mathbf{1}_B$; 0.5 equiv. of disordered toluene in the crystal lattice). Selected bond lengths, angles and dihedral angles of both molecules are given in Table 3. The complete set of structural data of **1**·bipy·$\mathbf{1}_A$ and **1**·bipy·$\mathbf{1}_B$ is available on request.[42]

Since both molecules **1**·bipy·$\mathbf{1}_A$ and **1**·bipy·$\mathbf{1}_B$ possess rather similar structures within experimental error, only

Figure 4. Molecular structure of **1**·bipy·$\mathbf{1}_A$; the thermal ellipsoids are drawn at a 50% probability level

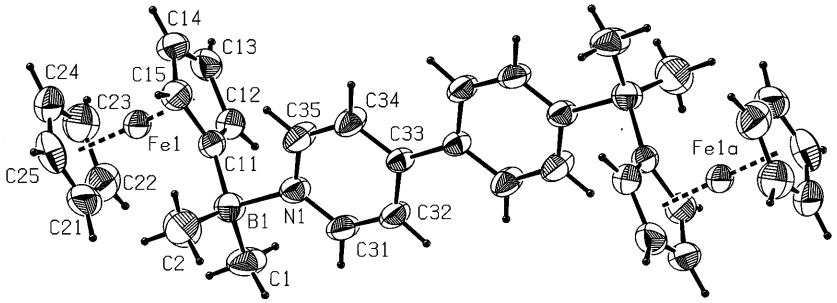

Table 2. Summary of crystallographic data of **1**·bipy·**1**

Formula	$C_{34}H_{38}B_2Fe_2N_2$
Form. wt.	608.00
Cryst. dimen. [mm]	0.20 × 0.13 × 0.13
Cryst. syst.	triclinic
Space group	*P*1 (No. 2)
T [K]	293
a [Å]	8.7143(5)
b [Å]	13.8257(10)
c [Å]	15.8214(12)
α [°]	65.820(7)
β [°]	86.337(7)
γ [°]	75.376(7)
V [Å^3]	1680.9(2)
$D_{calcd.}$ [g·cm^{-3}]	1.201
Z	2
Radiation	Mo-K_α, 0.71073 Å
Total reflns.	19554
No. of uniq. reflns.	5965
No. of obsd. reflns.	4982 [all data]
No. of parameters	361
μ [cm^{-1}]	8.9
Final *R1*[a]	0.0319 [$I > 2\sigma(I)$]
Final *wR2*[b]	0.0558 [all data]
GooF[c]	0.72

[a] $R1 = \Sigma(||F_o| - |F_c||)/\Sigma|F_o|$. – [b] $wR2 = [\Sigma w (F_o^2 - F_c^2)^2/\Sigma w (F_o^2)^2]^{1/2}$. – [c] $GooF = [\Sigma w (F_o^2 - F_c^2)^2/(NO - NV)]^{1/2}$.

Table 3. Selected bond lengths [Å], angles and torsion angles [°] of **1**·bipy·$\mathbf{1}_A$ and **1**·bipy·$\mathbf{1}_B$

	1·bipy·$\mathbf{1}_A$	**1**·bipy·$\mathbf{1}_B$
B(1)−N(1)	1.682(5)	1.689(4)
B(1)−C(11)	1.617(4)	1.604(5)
N(1)−C(31)	1.334(3)	1.339(4)
N(1)−C(35)	1.339(4)	1.323(4)
C(31)−C(32)	1.359(4)	1.366(5)
C(32)−C(33)	1.389(4)	1.378(5)
C(33)−C(34)	1.380(3)	1.381(4)
C(34)−C(35)	1.355(4)	1.370(4)
C(33)−C(33a)	1.480(4)	1.479(4)
C(1)−B(1)−N(1)	107.5(3)	104.8(2)
C(2)−B(1)−N(1)	103.9(3)	104.5(2)
C(11)−B(1)−N(1)	103.7(3)	104.1(3)
C(1)−B(1)−C(2)	113.5(3)	114.6(3)
C(1)−B(1)−C(11)	112.9(3)	113.1(3)
C(2)−B(1)−C(11)	114.2(3)	114.2(3)
B(1)−N(1)−C(31)	122.9(2)	120.4(3)
B(1)−N(1)−C(35)	121.0(2)	123.6(2)
C(12)−C(11)−B(1)−N(1)	90.5(4)	88.6(3)
C(11)−B(1)−N(1)−C(35)	42.9(4)	4.3(3)
C(34)−C(33)−C(33a)−C(34a)	180.0(7)	180.0(2)

1·bipy·$\mathbf{1}_A$ is discussed here in detail. As has already been deduced from the NMR data, the compound consists of two ferrocenylborane moieties bridged by a doubly coordinating bipy ligand. An inversion centre is located between C(33) and C(33a), and the bipy unit adopts the planar conformation required for an effective viologen-like electron acceptor. This finding is somewhat peculiar, because 4,4′-bipyridines, as well as biphenyls, tend to be twisted about their central C−C bond so as to minimize non-bonding interactions between adjacent hydrogen atoms.[43]

Compared to pyridine (py) complexes of boron Lewis acids,[43] the boron−nitrogen bonds of **1**·bipy·$\mathbf{1}_A$ are rather long [B(1)−N(1) = 1.682(5) Å; cf. BF_3·py: B−N = 1.603(5) Å, BCl_3·py: B−N = 1.592(3) Å].[38][44] Nevertheless, the boron centres are fully pyramidalized with the relevant angles C(1)−B(1)−C(2) = 113.5(3)°, C(1)−B(1)−C(11) = 112.9(3)° and C(2)−B(1)−C(11) = 114.2(3)° being only slightly larger than the value expected for an sp^3-hybridized boron atom with ideal tetrahedral geometry (109.5°). The B−N vectors of **1**·bipy·$\mathbf{1}_A$ are almost orthogonal to the C_5H_4 rings of the pendant ferrocenyl substituents with a torsion angle C(12)−C(11)−B(1)−N(1) of 90.5(4)°. The plane of the bipy bridge in **1**·bipy·$\mathbf{1}_A$ shows a dihedral angle C(11)−B(1)−N(1)−C(35) of 42.9(4)° with respect to the B(1)−C(11) bond [**1**·bipy·$\mathbf{1}_B$ shows a significantly different value of 4.3(3)°]. In summary, crystalline **1**·bipy·**1** features the desired molecular architecture: Two electropositive ferrocenyl fragments are held in close proximity to a rigid electroactive linker by means of simple B−N adduct formation.

Electrochemistry

The potential values are referred to the Saturated Calomel Electrode (S.C.E.); where necessary, literature data used for comparison have been recalculated for S.C.E. as reference. All the ferrocene adducts studied here display the typical ferrocene-centred oxidation, showing features of chemical reversibility on the cyclic voltammetric time scale. However, the electrochemical behaviour of most of the present complexes was found to be dependent on the concentrations employed. This is illustrated in Figure 5, which shows the cyclic voltammetric responses of **1**·bipy-Pr in DMF at concentrations of 2.3 × 10^{-3} mol·dm^{-3} (Figure 5a) and 0.2 × 10^{-3} mol·dm^{-3} (Figure 5b).

Following the main oxidation step, a minor but significant reversible peak system appears in the more dilute

sample at about +0.5 V, which vanishes almost completely when the concentration of **1**·bipy-Pr is increased by one order of magnitude. This picture is qualitatively independent of the scan rate (0.02 Vs^{-1} to 2.00 Vs^{-1}). **1**·bipy-Pr, as well as most other bipy adducts under investigation here, also exhibits two sequential reversible reduction processes, which are most likely centred at the bipy ligand ($E^{\circ\prime}$ = −0.80 V, −1.33 V; Table 4). Again, a concentration-dependent chemical complication is readily detectable. The corresponding potential value ($E^{\circ\prime} \approx -0.9$ V) is intermediate between the formal electrode potentials of the first redox transition of bipy ($E^{\circ\prime}$ = −1.84 V; Table 4) and that of paraquat $\mathbf{D}^{2+}$ ($E^{\circ\prime}$ = −0.36 V; Table 4). Moreover, the feature occurs at a more negative electrode potential than is observed in the case of **1**·bipy-Pr and may thus be assigned to the reduction of uncomplexed $[bipy\text{-}Pr]^+$. This assumption was confirmed by investigating an authentic sample of $[bipy\text{-}Pr]PF_6$, which possesses redox potentials of $E^{\circ\prime}$ = −0.95 V and −1.66 V. Our attempts to obtain cyclic voltammograms of **1** suffered from poor reproducibility due to severe decomposition processes that accompanied the one-electron removal. The minor reversible oxidation wave at $E^{\circ\prime} \approx +0.5$ V is thus probably not attributable to a $\mathbf{1}/\mathbf{1}^+$ transition, but may be tentatively assigned to the oxidation of parent ferrocene, formed by rapid decomposition of free **1** under the experimental conditions employed. It may be concluded, therefore, that the chemical complications observed at low concentrations of **1**·Do are indicative of a dynamic equilibrium between the B−N adducts and their constituent components, as has already been deduced from NMR and IR data.

Controlled potential coulometric tests performed on concentrated DMF solutions of **1**·bipy-Pr (E_w = +0.4 V) consume one electron per molecule. The colour of the solution turns to pale-green and the typical absorption (λ_{max} = 635 nm) of ferricinium derivatives is observed. Moreover, in confirmation of the chemical reversibility of the **1**·bipy-Pr/$[\mathbf{1}\cdot bipy\text{-}Pr]^+$ oxidation, cyclic voltammetry on the exhaustively oxidized solution gives a voltammetric profile quite complementary to that shown in Figure 5a.

Analysis[45] of the cyclic voltammetric anodic response with scan rates varying from 0.02 Vs^{-1} to 1.00 Vs^{-1} shows that (a) the current ratio i_{pc}/i_{pa} is equal to 1 throughout; (b) the current function $i_{pa}/v^{1/2}$ remains constant; (c) the peak-to-peak separation does not depart appreciably from the value of 59 mV theoretically expected for an electrochemically reversible one-electron process. The same diagnostic criteria essentially hold for both reduction steps. The electrochemical reversibility of these processes indicates that no significant structural reorganizations are involved. The relevant redox potentials are compiled in Table 4, together with the electrochemical characteristics of all other complexes under consideration.

In confirmation of the assumption that the oxidation process is centred on the ferrocene moiety and that the sequential reductions are centred on the bipy fragment, the relative peak heights of the cathodic vs. the anodic steps exactly reflect the ratio between the number of bipy and

Figure 5. Cyclic voltammetric responses recorded at a platinum electrode of DMF solutions containing $[NEt_4]PF_6$ (0.1 mol·dm^{-3}) and **1**·bipy-Pr: (a) 2.3 × 10^{-3} mol·dm^{-3}; (b) 0.2 × 10^{-3} mol·dm^{-3}; scan rate 0.2 Vs^{-1}

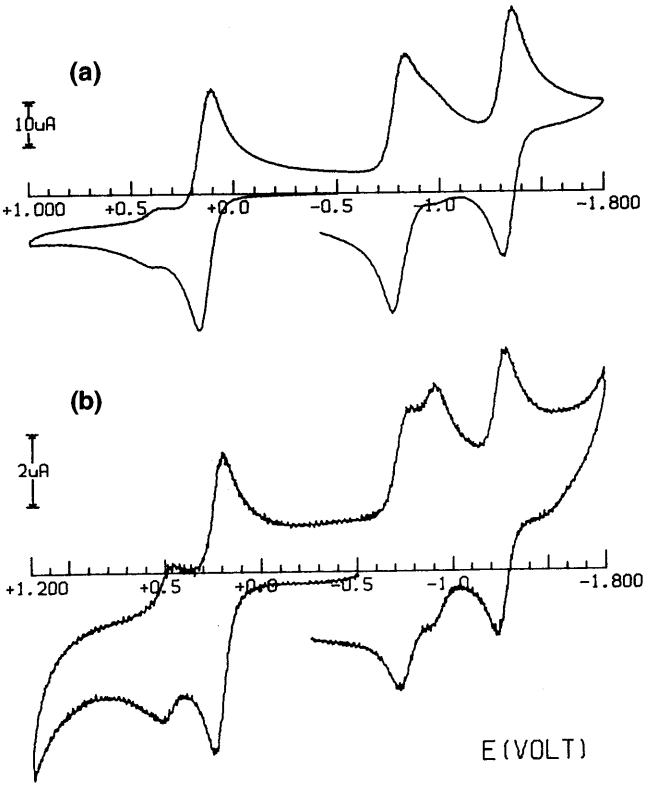

ferrocenyl units present in each molecule [i.e. **1**·bipy·**1**: 2:1; **2**·$(bipy\text{-}Pr)_2$: 1:2]. In passing, we note that the appearance of a single two-electron oxidation in the biferrocenyl complexes **1**·bipy·**1** and **1**·pyetpy·**1** suggests that no electronic communication between the outer ferrocenyl fragments takes place.

The presence of four-coordinate boron substituents in **1**·Do and **2**·$(Do)_2$ considerably lowers the oxidation potential of the central iron atoms. The effect is apparently additive, as can be seen from the $E^{\circ\prime}$ values of the parent ferrocene (+0.49 V), **1**·pic (+0.20 V) and **2**·$(pic)_2$ (−0.01 V) in DMF solution (Table 4). Oxidation generally occurs at somewhat more cathodic values in CH_2Cl_2. Most importantly, the oxidation potentials of **1**·pic ($E^{\circ\prime}$ = +0.20 V [DMF], +0.11 V [CH_2Cl_2]) and **2**·$(pic)_2$ ($E^{\circ\prime}$ = −0.01 V [DMF], −0.12 V [CH_2Cl_2]) are very close to those of Cp* FeCp ($E^{\circ\prime}$ = +0.12 [CH_3CN])[46] and Cp*FeCp* ($E^{\circ\prime}$ = −0.12 [CH_3CN]),[46] respectively. When pic is substituted by the more nucleophilic DMAP, a cathodic shift of the Fe^{II}/Fe^{III} transition is observed: $\Delta E^{\circ\prime}$(**1**·DMAP − **1**·pic) = −0.05 V [CH_2Cl_2], $\Delta E^{\circ\prime}$[**2**·$(DMAP)_2$ − **2**·$(pic)_2$] = −0.08 V [CH_2Cl_2]. We may therefore conclude that the electron-donating ability of a BMe_2·Do substituent attached to the Cp ligand is approximately equal to the positive inductive effect of the five methyl groups in (pentamethyl)cyclopentadienyl (Cp*). In addition, some fine-tuning of the Fe^{II}/Fe^{III} redox potential is possible by choosing pyridine bases of different pK_a values for boron coordination.

Table 4. Electrochemical and spectroscopic data characterizing the redox changes exhibited by the B−N adducts under study; formal electrode potentials $E^{\circ\prime}$ in V, vs. S.C.E.; peak-to-peak separations ΔE_p in mV, at 0.2 Vs^{-1}; wavelengths λ_{max} in nm for the oxidized ferricinium species

	$E^{\circ\prime}_{ox}$ (ΔE_p)	λ_{max}[a]	$E^{\circ\prime}_{red1}$ (ΔE_p)	$E^{\circ\prime}_{red2}$ (ΔE_p)	Solvent
1·pic	+0.20 (72)	[b]	–	–	DMF
	+0.11 (132)	[b]	–	–	CH_2Cl_2
1·DMAP	+0.18 (72)	[c]	–	–	DMF
	+0.06 (83)	648	–	–	CH_2Cl_2
1·bipy-Pr	+0.14 (76)	635	−0.80 (80)	−1.33 (62)	DMF
	+0.19 (96)	[b]	−0.78 (63)	−1.40 (71)	CH_2Cl_2
2·$(pic)_2$	−0.01 (73)	[c]	–	–	DMF
	−0.12 (121)	640	–	–	CH_2Cl_2
2·$(DMAP)_2$	−0.10 (73)	[c]	–	–	DMF
	−0.20 (86)	641	–	–	CH_2Cl_2
2·$(bipy\text{-}Pr)_2$	+0.02 (114)	[b]	−0.74 (89)	−1.30 (65)	DMF
	[d]	–	[d]	[d]	CH_2Cl_2
1·bipy·**1**	+0.17 (66)	[c]	−1.20 (72)	−1.75 (60)	DMF
	+0.15 (80)	627	−1.37 (128)	−1.91[e]	CH_2Cl_2
1·pyetpy·**1**	+0.21 (71)	[c]	–	–	DMF
	+0.11 (79)	630	–	–	CH_2Cl_2
bipy[f]	–	–	−1.84	−2.38	DMF
$\mathbf{D}^{2+}$[f]	–	–	−0.36	−0.80	DMF
FcH	+0.49 (72)	–	–	–	DMF
	+0.44 (90)	620	–	–	CH_2Cl_2

[a] Referred to the oxidized species. – [b] Not measured because of slow decomposition. – [c] Not measured. – [d] Not interpretable. – [e] Peak potential value. – [f] Ref.[6].

As expected, B−N adduct formation shifts the two reduction potentials of the bipy moiety by more than 0.6 V (DMF) towards more anodic values in the dimetallic complex **1**·bipy·**1** (bipy: $E^{\circ\prime}$ = −1.84 V, −2.38 V;[36] **1**·bipy·**1**: $E^{\circ\prime}$ = −1.20 V, −1.75 V). This effect is somewhat less pronounced than in the 9-boraadamantane adduct **C** [Figure 2; $E^{\circ\prime}$ = −1.10 V, −1.68 V (DMSO)],[36] which may be explained by the lower Lewis acidity of **1** bearing a strongly electron-donating ferrocenyl substituent. Like the Fc fragments in **1**·bipy·**1**, the two bipy-Pr substituents in **2**·$(bipy\text{-}Pr)_2$ do not show any significant degree of electronic communication.

UV/Vis Spectroscopy

In the solid state, all bipy complexes **1**·bipy·**1**, **1**·bipy-Pr, **2**·$(bipy\text{-}Pr)_2$ and [**2**·bipy]$_n$ exhibit an intense blue to purple colour, and single crystals of these compounds are almost black. We consider that these additional electronic absorptions, which cannot be attributed to internal transitions of bipy or the ferrocenylboranes **1** and **2**, are due to charge-transfer interactions between the electron-rich ferrocene donors and the electron-poor bipy diadducts. When the extended π-electron system of bipy is disrupted by inserting an ethylene spacer into its central C−C bond, the viologen-like electron acceptor is destroyed, and consequently the colour of the respective complexes changes to yellow (cf. **1**·pyetpy·**1**, [**2**·pyetpy]$_n$).

Somewhat surprisingly, the UV/Vis spectra of **1**·bipy·**1** and **1**·pyetpy·**1** are rather similar in solution (toluene, CH_2Cl_2) [λ_{max} = 447 nm (**1**·bipy·**1**); 447 nm (**1**·pyetpy·**1**)]. Several possible explanations for this phenomenon can be envisaged: (a) The Fc-to-bipy charge transfer may occur *inter*molecularly and thus require close contacts with specific spatial orientation of the individual complexes. These conditions are more likely to be met in the solid state rather than in dilute solution. (b) As has been shown by X-ray crystallography, the bipy bridge of **1**·bipy·**1** adopts a planar conformation in the crystal lattice. In solution, however, rotation about the central C(33)−C(33a) bond is to be expected, leading to a weakening of the electron acceptor due to the continuous perturbation of the π-electron system. (c) The Lambert-Beer law is only valid for highly dilute solutions. Since dilution favours dissociation of **1**·bipy·**1** and **1**·pyetpy·**1**, the UV spectra recorded under these conditions are not representative of the adduct complexes, but are most likely dominated by the bands of free **1**, bipy and pyetpy.

Thermal Analysis

To investigate the stability of solid **1**·bipy·**1** and [**2**·bipy]$_n$ more closely, differential thermal scans (DSC)[47] and thermogravimetric measurements (TG-MS)[48] were performed [heating rate: 10 $K \cdot min^{-1}$; inert gas flow (He): 16 sccm (DSC); 60 sccm (TGA)]. For comparison, the model compounds **1**·pic, **1**·DMAP and **2**·$(pic)_2$, **2**·$(DMAP)_2$ were included in this study.

All complexes show a sharp endothermic feature, followed by a broad, sometimes ill-defined, endothermic event at higher temperatures. With the exception of **2**·$(pic)_2$, the position of the first signal is independent of whether the thermal scans are run at constant pressure or at constant volume. In contrast, the second endothermic transition is markedly influenced by pressure and its onset temperature is generally shifted to higher values in a closed system (V = const.; Table 5).

These findings suggest that the first signal in each DSC plot is due to crystal melting, and this was confirmed by independent melting-point determinations, during which

Table 5. Results of DSC measurements

	1·pic	**1**·DMAP	**2**·$(pic)_2$	**2**·$(DMAP)_2$	**1**·bipy·**1**	$[\mathbf{2}\cdot bipy]_n$
$T(1)_{on}$[a]	127[c]/128[d]	156[c]/156[d]	165[c]/198[d]	244[c]/250[d]	180[c]/180[d]	240[c]/240[d]
$T(1)_p$[b]	130[c]/132[d]	160[c]/163[d]	182[c]/202[d]	254[c]/256[d]	182[c]/184[d]	245[c]/247[d]
$T(2)_{on}$[a]	—[c]/—[d]	—[c]/290[d]	—[c]/—[d]	—[c]/296[d]	—[c]/284[d]	—[c]/—[d]
$T(2)_p$[b]	195[c]/240[d]	290[c]/320[d]	—[c]/250[d]	280[c]/310[d]	240[c]/305[d]	260[c]/—[d]

[a] Onset temperature. — [b] Peak temperature of the first (1) and second (2) endothermic events. — [c] p = constant. — [d] V = constant.

the samples were viewed under a microscope. The much broader, less regular line shape recorded in most cases for the second endotherm, as well as its pressure dependence, indicates the occurrence of chemical transformations in the respective temperature range. At this stage, B−Cp and B−N bond rupture takes place, generating more volatile components such as the free pyridine bases, ferrocene, and the $(C_5H_5)Fe$ fragment (cf. $[\mathbf{2}\cdot bipy]_n$; Figure 6). The melting process of some adducts is thus accompanied by chemical decomposition. In these cases, it is not possible to accurately determine the onset temperatures $T(2)_{on}$ and therefore only the peak values $T(2)_p$ are given in Table 5. The melting points of **1**·pic to **2**·$(DMAP)_2$ show the expected influence of base strength, dipole moment, and molecular weight of the individual compounds. On going from pic to the more basic DMAP, the decomposition temperatures increase, which provides additional support for the assumption that the B−N bonds are the weakest parts in the molecular frameworks. No significant differences are found for the decomposition temperatures $T(2)_p$ of **1**·pic, **2**·$(pic)_2$ on the one hand, and of **1**·DMAP, **2**·$(DMAP)_2$ on the other. Hence, B−N adduct formation at one BMe_2 substituent seems to have little influence on the Lewis acidity of the second boron centre.

The dimetallic complex **1**·bipy·**1** and the coordination polymer $[\mathbf{2}\cdot bipy]_n$ possess high thermal stability in the solid state (Table 5). This finding is in contrast to the ready dissociation of $[\mathbf{2}\cdot bipy]_n$, even at moderate temperatures in toluene: As outlined above, $[\mathbf{2}\cdot bipy]_n$ is virtually insoluble in all common solvents at 20°C. At elevated temperature (T > 85°C), however, a slurry of $[\mathbf{2}\cdot bipy]_n$ in toluene is turned into a clear, orange-red solution, from which purple dendritic crystals are re-formed upon cooling (T < 70°C). This process may be repeated several times without significant decomposition of the material. The thermal behaviour of $[\mathbf{2}\cdot bipy]_n$ in the presence of a low-polarity solvent indicates that a reversible rupture of the oligomer backbone can be induced. Thermolysis of a slurry of $[\mathbf{2}\cdot bipy]_n$ in anhydrous and deaerated $[D_8]$toluene was also monitored by means of ^{1}H-NMR spectroscopy. Initially (20°C), the colourless supernatant shows no signals other than those of incompletely deuterated solvent. Upon heating to 80°C, however, resonances attributable to the mononuclear building blocks **2** [$\delta(^1H)$ = 0.84, 4.31, 4.44] and bipy [($\delta(^1H)$ = 7.51, 8.72]

Figure 6. DSC, TG/DTG plots of $[\mathbf{2}\cdot bipy]_n$ and mass spectrometric analysis of thermolysis products

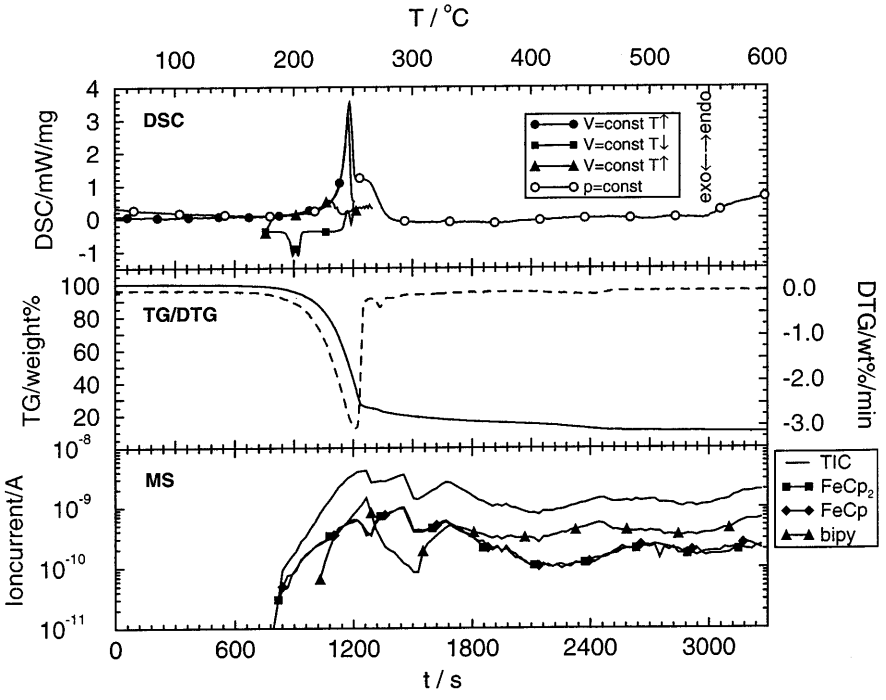

are detected in a molar ratio of 1:1. Some reversibility of the thermal transformation of [**2**·bipy]$_n$ is also maintained in the solid state (Figure 6).

When heating of the sample is stopped at 250°C under isochoric conditions and then the sample is cooled down again, an exothermic event is observed with an onset temperature $T(2)_{on}$ = 207°C and a peak temperature $T(2)_p$ = 200°C. A second heating scan again reveals an endothermic transition [$T(2)_p$ = 220°C] of lower intensity compared to the first scan.

Polymer Analysis

IR spectroscopy, DSC measurements and elemental analysis of neat [**2**·bipy]$_n$ suggest that this material consists of B−N coordination polymers. A solid-state ^{13}C-NMR spectrum of [**2**·bipy]$_n$ reveals that the compound crystallizes together with a small proportion of toluene. Otherwise, only the signals expected for well-defined polymeric [**2**·bipy]$_n$ are observed [$\delta(^{13}C)$ = 13.7 (BMe), 71.5 (Fc), 90.3 (Fc-*ipso*), 121.7, 143.9 (bipy), 147.2 (bipy-*ipso*)].

When a slurry of purple [**2**·bipy]$_n$ in CH_2Cl_2 is treated with excess pic, a clear orange solution is obtained (cf. Scheme 2), from which **2**·(pic)$_2$ and free bipy can be recovered in almost quantitative yield. This finding clearly demonstrates that the integrities of the molecular frameworks of **2** and bipy are maintained in [**2**·bipy]$_n$, and that its formation is not accompanied by unwanted side reactions. Moreover, it is evident that the copolymerization of **2** and bipy can not only be reversed by thermally induced B−N bond cleavage (see above), but also with the help of Lewis basic additives.

We have attempted to gather more detailed structural information on [**2**·bipy]$_n$ by X-ray crystallography. Unfortunately, we have not yet been able to obtain single crystals of sufficiently good quality to allow a full structure refinement (polysynthetic twins), although the polymeric nature of [**2**·bipy]$_n$ has been proven by a preliminary crystal structure solution.

Conclusion

A boron−nitrogen donor−acceptor bond is highly directional and is of a reversible nature. It can be very strong (H_3B-NH_3: 31 kcal·mol^{-1}), but the energy required for heterolytic dissociation may also be tuned over a wide range by judicious choice of appropriate substituents at the boron and nitrogen atoms. We therefore suggest consideration of B−N Lewis acid/base pairing as an alternative to hydrogen bonding for the generation of reversible polymer systems. Since an individual hydrogen bond is rather weak (3−7 kcal·mol^{-1}), only the cooperative action of many of them provides a linker that is sufficiently stable to build well-defined supramolecular aggregates.[49] The efficient control of cooperative phenomena requires very careful positioning of every single binding site, and this difficult task can be circumvented by employing B−N bonds instead.

On the basis of this B−N concept, organometallic polymers [**2**·bipy]$_n$ and [**2**·pyetpy]$_n$ have been synthesized from 1,1′-fc(BMe$_2$)$_2$, **2**, 4,4′-bipyridine, and 1,2-bis(4-pyridyl)-ethane, respectively. Neat [**2**·bipy]$_n$ is stable up to 240°C in the solid state. In the presence of toluene, however, the polymer is reversibly split into its constituent monomers upon warming to 85°C.

Apart from its role in establishing the polymer backbone, B−N adduct formation substantially changes the charge distribution of the ferrocene fragments and of the bipy bridges, as is evident from an investigation of the model complexes **1**·Do, **2**·(Do)$_2$ [Do: γ-picoline, 4-(dimethylamino)pyridine, *N*-(*n*-propyl)-4-(4′-pyridyl)pyridinium hexafluorophosphate], and **1**·Do·**1** [Do: 4,4′-bipyridine, 1,2-bis(4-pyridyl)ethane]: The donor strength of one BMe$_2$·Do substituent at ferrocene is equal to the electron-releasing effect of five methyl groups and consequently leads to a large cathodic shift of the Fe^{II}/Fe^{III} redox transition {e.g. $E^{\circ\prime}$ = +0.44 V [CpFeCp, CH_2Cl_2]; +0.11 V [**1**·pic, CH_2Cl_2], +0.12 V [Cp*FeCp, CH_3CN]; −0.12 V [**2**·(pic)$_2$, CH_2Cl_2], −0.12 V [Cp*FeCp*, CH_3CN]}. For this reason, base adducts of ferrocenylboranes are an alternative to the widely used decamethylferrocene as electron donors in organometallic redox chemistry. In contrast to Cp*FeCp*, there are still four CH groups at each Cp ring of **1**·Do and **2**·(Do)$_2$ available for further functionalization, and the Fe^{II}/Fe^{III} redox potential is, moreover, tunable by selecting the appropriate pyridine base.

The electrochemical behaviour of the bipy linker is also sensitive to its coordination state, since each of the two one-electron reductions of parent 4,4′-bipyridine ($E^{\circ\prime}$ = −1.84 V, −2.38 V; DMF) is shifted by about 0.6 V towards less negative values as a result of FcBMe$_2$ binding ($E^{\circ\prime}$ = −1.20 V, −1.75 V [**1**·bipy·**1**; DMF]).

Destabilization of the ferrocene HOMO parallel to the stabilization of the bipy LUMO facilitates charge-transfer interactions between the two orbitals in **1**·bipy·**1**, **1**·bipy-Pr, **2**·(bipy-Pr)$_2$ and [**2**·bipy]$_n$, as indicated by the deep-purple colour of these compounds. In contrast, the ferrocene-free B−N adducts **C** (Figure 2), as well as the metal-containing complexes **1**·pyetpy·**1** and [**2**·pyetpy]$_n$ with two separated pyridine rings, exhibit the yellow colour usually observed for ferrocene derivatives bearing tetracoordinate boron substituents. The question as to whether charge-transfer in e.g. [**2**·bipy]$_n$ occurs within the polymeric rod or between two adjacent polymer chains will be subject of future investigations. Also attendant on the investigation of [**2**·bipy]$_n$ is the screening of a variety of bidentate Lewis bases other than bipy in order to increase the extent of charge delocalization in ferrocenylborane-containing coordination polymers. Promising results have already been obtained with pyrazine, which (a) brings adjacent ferrocene units into closer proximity, (b) is more rigid than bipy, and (c) forms bis-quaternary salts that are able to accept an electron at considerably more anodic potential values compared to *N*,*N*′-dialkylbipyridinium acceptors.[50][51]

We are grateful to Prof. Dr. *W. A. Herrmann* (Technische Universität München) for his generous support, to *H. Heise* for recording the solid-state ^{13}C-NMR spectra, and to *W. Hieringer* for helpful discussions. Financial funding by the *Deutsche Forschungsgemein-*

schaft (DFG) and the *Fonds der Chemischen Industrie* is acknowledged.

Experimental Section

All reactions and manipulations were carried out in dry, oxygen-free Ar using standard Schlenk glassware or in an Ar-filled dry-box. Solvents were freshly distilled under N_2 from Na/K alloy/benzophenone (hexane, toluene, THF) or from CaH_2 (CH_2Cl_2, CH_3Cl, CH_3CN) prior to use. − UV/Vis: Hewlett-Packard 8452 A. − IR: Perkin-Elmer 1650 FT-IR. − NMR: Jeol JMN-GX 400 and Bruker DPX 400 [abbreviations: s: singlet, d: doublet, t: triplet, vt: virtual triplet, br: broad, n.r.: multiplet expected but not resolved; pic: γ-picoline, DMAP: 4-(dimethylamino)pyridine, bipy: 4,4′-bipyridine, pyetpy: 1,2-bis(4-pyridyl)ethane, bipy-Pr: *N*-(*n*-propyl)-4-(4′-pyridyl)pyridinium hexafluorophosphate]. − ^{11}B-NMR spectra were referenced to external $BF_3{\cdot}Et_2O$. − MS (FAB/CI mode): Finnigan MAT 90. − Thermal analyses: Netzsch DSC 404 high-temperature furnace, thermocouple Pt/Rh, Perkin-Elmer TGA 7 thermobalance equipped with a Balzers QMG 420 mass spectrometer. − Elemental analyses: Microanalytical laboratory of the Technische Universität München. − The compounds **1**, **2**[15] and bipy-Pr[26] were synthesized according to literature procedures.

Preparation of **1**·pic: To a solution of **1** (0.25 g, 1.11 mmol) in toluene (10 ml) at ambient temperature, was added γ-picoline (0.10 g, 1.07 mmol) in toluene (5 ml) by means of a cannula. The resultant clear orange solution was stirred for 3 h and then concentrated to half of its original volume in vacuo, whereupon **1**·pic gradually precipitated as an orange crystalline solid. The precipitate was collected on a frit (G3), treated with cold hexane (−30°C) and dried in vacuo. The mother liquor was kept in a refrigerator (−30°C) for 12 h to yield a second crop. Yield 0.32 g (93%). − IR (KBr, cm^{-1}): $\tilde{\nu}$ = 1628 (vs), 1507 (m) (pic-C−C, C−N), 1104 (m), 1068 (m), 1058 (m) (B−N). − ^{11}B NMR (128.3 MHz, $CDCl_3$): δ = 0.4 ($h_{1/2}$ = 300 Hz). − ^{1}H NMR (400 MHz, $CDCl_3$): δ = 0.27 (s, 6 H, BCH_3), 2.35 (s, 3 H, pic-CH_3), 4.03 (vt, 2 H, *J* = 1.7 Hz, C_5H_4), 4.06 (s, 5 H, C_5H_5), 4.16 (vt, 2 H, *J* = 1.7 Hz, C_5H_4), 7.16 (d, 2 H, *J* = 6.6 Hz, pic-3-H, -5-H), 8.41 (d, 2 H, *J* = 6.6 Hz, pic-2-H, -6-H). − ^{13}C NMR (100.5 MHz, $CDCl_3$): δ = 11.1 (br, BCH_3), 21.0 (pic-CH_3), 67.9 (C_5H_5), 68.4, 71.7 (C_5H_4), n.o. (C_5H_4-*ipso*), 125.4 (pic-C-3, -C-5), 144.5 (pic-C-2, -C-6), 150.7 (pic-C-4). − $C_{18}H_{22}BFeN$ (319.04): calcd. C 67.77, H 6.95, N 4.39; found C 67.86, H 6.92, N 4.31.

Preparation of **1**·DMAP: **1** (0.34 g, 1.51 mmol) in toluene (10 ml) was treated with 4-(dimethylamino)pyridine (0.18 g, 1.47 mmol) in toluene (5 ml) at ambient temperature. The cloudy orange mixture was stirred for 1 h and then concentrated to half of its original volume in vacuo, whereupon an orange precipitate gradually formed. The precipitate was removed by filtration (G3 frit), triturated with hexane, and dried in vacuo. A second crop was obtained from the mother liquor upon storage at −30°C for 12 h. Yield 0.46 g (90%). − IR (KBr, cm^{-1}): $\tilde{\nu}$ = 1636 (vs), 1544 (m) (DMAP-C−C, C−N), 1104 (m), 1076 (m), 1058 (m) (B−N). − ^{11}B NMR (128.3 MHz, $CDCl_3$): δ = −3.0 ($h_{1/2}$ = 300 Hz). − ^{1}H NMR (400 MHz, $CDCl_3$): δ = 0.16 (s, 6 H, BCH_3), 3.02 (s, 6 H, NCH_3), 3.97 (vt, 2 H, *J* = 1.5 Hz, C_5H_4), 4.05 (s, 5 H, C_5H_5), 4.09 (vt, 2 H, *J* = 1.5 Hz, C_5H_4), 6.41 (d, 2 H, *J* = 6.6 Hz, DMAP-3-H, -5-H), 8.09 (d, 2 H, *J* = 6.6 Hz, DMAP-2-H, -6-H). − ^{13}C NMR (100.5 MHz, $CDCl_3$): δ = 10.9 (br, BCH_3), 39.2 (NCH_3), 67.8 (C_5H_5), 68.0, 71.5 (C_5H_4), n.o. (C_5H_4-*ipso*), 106.0 (DMAP-C-3, -C-5), 144.2 (DMAP-C-2, -C-6), 154.4 (DMAP-C-4). − $C_{19}H_{25}BFeN_2$ (348.08): calcd. C 65.56, H 7.24, N 8.05; found C 65.28, H 7.16, N 7.96.

Preparation of **1**·bipy-Pr: **1** (0.11 g, 0.49 mmol) in CH_3CN (3 ml) was treated with *N*-(*n*-propyl)-4-(4′-pyridyl)pyridinium hexafluorophosphate (0.17 g, 0.49 mmol) in CH_3CN (2 ml) at ambient temperature. The reaction mixture, which instantaneously took on a purple colour, was stirred for 1 h and then concentrated to a volume of 1 ml. Toluene (15 ml) was added, whereupon **1**·bipy-Pr precipitated quantitatively as a dark-purple microcrystalline solid, which was triturated with toluene (3 × 5 ml) and hexane (2 × 5 ml) and dried in vacuo overnight. Yield 0.25 g (90%). − IR (KBr, cm^{-1}): $\tilde{\nu}$ = 1646 (vs), 1627 (vs), 1552 (m), 1501 (m) (bipy-C−C, C−N), 1102 (m), 1079 (m), 1061 (m) (B−N). − ^{11}B NMR (128.3 MHz, CD_3CN): δ = 7.5 ($h_{1/2}$ = 350 Hz). − ^{1}H NMR (400 MHz, CD_3CN): δ = 0.30 (s, 6 H, BCH_3), 0.97 (t, 3 H, *J* = 7.5 Hz, CH_3), 2.01 (m, 2 H, CH_2CH_3), 4.06 (s, 5 H, C_5H_5), 4.08, 4.19 (n.r., 2 × 2 H, C_5H_4), 4.53 (t, 2 H, *J* = 7.6 Hz, NCH_2), 7.91, 8.29, 8.80, 8.87 (4 × d, 4 × 2 H, *J* = 6.5 Hz, bipy). − ^{13}C NMR (100.5 MHz, CD_3CN): δ = 10.5 (CH_3), 11.0 (br, BCH_3), 25.3 (CH_2CH_3), 64.0 (NCH_2), 69.2 (C_5H_5), 70.0, 72.5 (2 × br, C_5H_4), n.o. (C_5H_4-*ipso*), 124.4, 127.7, 144.6, 146.1, 148.5, 153.5 (bipy). − $C_{25}H_{30}BF_6FeN_2P$ (570.15): calcd. C 52.67, H 5.30, N 4.91; found C 52.33, H 5.25, N 4.92.

Preparation of **1**·bipy·**1**: At ambient temperature, a colourless solution of 4,4′-bipyridine (0.25 g, 1.60 mmol) in toluene (10 ml) was added dropwise to an orange-red solution of **1** (0.73 g, 3.23 mmol) in toluene (10 ml). The reaction mixture, which instantaneously took on a dark-brown colour, was stirred for 3 h, whereupon a purple microcrystalline solid gradually precipitated. All insolubles were collected on a frit (G3), triturated with toluene (5 ml) and hexane (5 ml), and dried in vacuo. The filtrate was kept at −30°C overnight to yield a second crop. Yield 0.91 g (94%). X-ray quality crystals were obtained from toluene/hexane (1:1) at −30°C. − IR (KBr, cm^{-1}): $\tilde{\nu}$ = 1622 (vs), 1540 (m), 1493 (m) (bipy-C−C, C−N), 1100 (s), 1075 (s), 1058 (s) (B−N); IR (CH_2Cl_2, cm^{-1}): $\tilde{\nu}$ = 1622 (vs), 1597 (w), 1538 (w), 1517 (vw), 1489 (m) (bipy-C−C, C−N), 1104 (s), 1076 (s), 1058 (s) (B−N). − UV (CH_2Cl_2): λ = 239, 447 nm. − ^{11}B NMR (128.3 MHz, $CDCl_3$): δ = 15.1 ($h_{1/2}$ = 700 Hz). − ^{1}H NMR (400 MHz, $CDCl_3$): δ = 0.40 (s, 12 H, BCH_3), 4.08 (s, 10 H, C_5H_5), 4.13, 4.27 (2 × n.r., 2 × 4 H, C_5H_4), 7.53 (d, 4 H, *J* = 5.5 Hz, bipy-3-H, -5-H), 8.72 (d, 4 H, *J* = 5.5 Hz, bipy-2-H, -6-H). − ^{13}C NMR (100.5 MHz, $CDCl_3$): δ = 10.8 (br, BCH_3), 68.5 (C_5H_5), 70.3, 72.8 (C_5H_4), n.o. (C_5H_4-*ipso*), 122.2 (bipy-C-3, -C-5), 145.9 (bipy-C-4), 147.4 (bipy-C-2, -C-6). − $C_{34}H_{38}B_2Fe_2N_2$ (608.00): calcd. C 67.17, H 6.30, N 4.61; found C 66.81, H 6.54, N 4.41.

Preparation of **1**·pyetpy·**1**: **1** (0.72 g, 3.19 mmol) in toluene (20 ml) was treated dropwise with 1,2-bis(4-pyridyl)ethane (0.29 g, 1.57 mmol) in toluene (10 ml) at ambient temperature. A yellow microcrystalline solid precipitated from the orange reaction mixture. The slurry was stirred for 3 h and the solid material was isolated by filtration. After trituration with toluene (5 ml) and hexane (5 ml), the product was dried in vacuo. Yield 0.96 g (84%). − IR (KBr, cm^{-1}): $\tilde{\nu}$ = 1623 (s), 1560 (w), 1506 (m), 1496 (m) (pyetpy-C−C, C−N), 1102 (m), 1069 (s), 1061 (m) (B−N). − UV (CH_2Cl_2): λ = 239, 447 nm. − ^{11}B NMR (128.3 MHz, $CDCl_3$): δ = 6.2 ($h_{1/2}$ = 900 Hz). − ^{1}H NMR (400 MHz, $CDCl_3$): δ = 0.29 (s, 12 H, BCH_3), 2.94 (s, 4 H, -CH_2-), 4.04 (vt, 4 H, *J* = 1.5 Hz, C_5H_4), 4.06 (s, 10 H, C_5H_5), 4.18 (vt, 4 H, *J* = 1.5 Hz, C_5H_4), 7.14 (d, 4 H, *J* = 6.0 Hz, pyetpy-3-H, -5-H), 8.48 (d, 4 H, *J* = 6.0 Hz, pyetpy-2-H, -6-H). − ^{13}C NMR (100.5 MHz, $CDCl_3$): δ = 10.9 (br, BCH_3), 34.8 (−CH_2−), 68.1 (C_5H_5), 69.2, 72.1 (C_5H_4), n.o. (C_5H_4-*ipso*), 124.4 (pyetpy-C-3, -C-5), 145.8 (pyetpy-C-2, -C-6), 151.8 (pyetpy-C-4). − $C_{36}H_{42}B_2Fe_2N_2$ (636.07)·C_7H_8 (92.14): calcd. C 70.92, H 6.92, N 3.85; found C 70.97, H 6.67, N 3.79.

Preparation of **2**·$(pic)_2$: **2** (0.43 g, 1.62 mmol) in toluene (10 ml) was treated with a solution of γ-picoline (0.33 g, 3.54 mmol) in

toluene (5 ml) at ambient temperature. The resultant orange slurry was stirred for 1 h. Insoluble material was collected on a frit (G3), triturated with hexane (5 ml), and dried in vacuo. Yield 0.59 g (81%). − IR (KBr, cm^{-1}): $\tilde{\nu}$ = 1628 (s), 1508 (m) (pic-C−C, C−N), 1066 (s), 1047 (s) (B−N). − ^{11}B NMR (128.3 MHz, $CDCl_3$): δ = 15.0 ($h_{1/2}$ = 300 Hz). − ^{1}H NMR (400 MHz, $CDCl_3$): δ = 0.34 (s, 12 H, BCH_3), 2.37 (s, 6 H, pic-CH_3), 3.99, 4.13 (2 × n.r., 2 × 4 H, C_5H_4), 7.15 (d, 4 H, J = 6.0 Hz, pic-3-H, -5-H), 8.44 (d, 4 H, J = 6.0 Hz, pic-2-H, -6-H). − ^{13}C NMR (100.5 MHz, $CDCl_3$): δ = 10.9 (br, BCH_3), 21.1 (pic-CH_3), 71.0, 72.6 (C_5H_4), n.o. (C_5H_4-*ipso*), 125.2 (pic-C-3, -C-5), 145.6 (pic-C-2, -C-6), 149.8 (pic-C-4). − $C_{26}H_{34}B_2FeN_2$ (452.04): calcd. C 69.08, H 7.58, N 6.20; found C 68.58, H 7.38, N 6.10.

Preparation of **2**·$(DMAP)_2$: The compound was synthesized similarly to **2**·$(pic)_2$ using **2** (0.18 g, 0.68 mmol) and 4-(dimethylamino)-pyridine (0.17 g, 1.39 mmol). Yield 0.28 g (81%). − IR (KBr, cm^{-1}): $\tilde{\nu}$ = 1638 (vs), 1552 (s) (DMAP-C−C, C−N), 1077 (m), 1060 (m) (B−N). − ^{11}B NMR (128.3 MHz, $CDCl_3$): δ = −2.3 ($h_{1/2}$ = 500 Hz). − ^{1}H NMR (400 MHz, $CDCl_3$, 55°C): δ = 0.39 (s, 12 H, BCH_3), 3.01 (s, 12 H, NCH_3), 4.01, 4.16 (2 × n.r., 2 × 4 H, C_5H_4), 6.42 (d, 4 H, J = 6.6 Hz, DMAP-3-H, -5-H), 8.12 (d, 4 H, J = 6.6 Hz, DMAP-2-H, -6-H). − ^{13}C NMR (100.5 MHz, $CDCl_3$, 55°C): δ = 10.6 (br, BCH_3), 39.2 (NCH_3), 71.8, 73.1 (C_5H_4), n.o. (C_5H_4-*ipso*), 106.1 (DMAP-C-3, -C-5), 144.4 (DMAP-C-2, -C-6), 154.7 (DMAP-C-4). − $C_{28}H_{40}B_2FeN_4$ (510.13): calcd. C 65.93, H 7.90, N 10.98; found C 65.44, H 7.77, N 10.74.

Preparation of **2**·$(bipy\text{-}Pr)_2$: The compound was synthesized similarly to **1**·bipy-Pr from **2** (0.19 g, 0.71 mmol) and *N*-(*n*-propyl)-4-(4′-pyridyl)pyridinium hexafluorophosphate (0.49 g, 1.42 mmol). Yield 0.42 g (60%). − IR (KBr, cm^{-1}): $\tilde{\nu}$ = 1645 (vs), 1624 (s), 1550 (m), 1496 (m), 1470 (m) (bipy-C−C, C−N), 1072 (w), 1062 (m) (B−N). − ^{11}B NMR (128.3 MHz, CD_3CN): δ = 15.1 ($h_{1/2}$ = 500 Hz). − ^{1}H NMR (400 MHz, CD_3CN): δ = 0.42 (br, 12 H, BCH_3), 0.97 (t, 6 H, J = 7.5 Hz, CH_3), 2.01 (m, 4 H, CH_2CH_3), 4.05, 4.18 (2 × n.r., 2 × 4 H, C_5H_4), 4.52 (t, 4 H, J = 7.6 Hz, NCH_2), 7.88, 8.30, 8.76, 8.88 (4 × d, 4 × 4 H, J = 6.5 Hz, bipy). − ^{13}C NMR (100.5 MHz, CD_3CN): δ = 10.5 (CH_3), 11.0 (br, BCH_3), 25.3 (CH_2CH_3), 64.0 (NCH_2), 73.0, 74.0 (2 × br, C_5H_4), n.o. (C_5H_4-*ipso*), 124.1, 127.4, 144.1, 146.0, 149.2, 153.9 (bipy). − $C_{40}H_{50}B_2F_{12}FeN_4P_2$ (954.27)·0.4 C_7H_8 (92.14): calcd. C 51.87, H 5.41, N 5.65, Fe 5.63; found C 51.92, H 5.45, N 5.68, Fe 5.23.

Preparation of [**2**·bipy]$_n$: A red solution of **2** (0.13 g, 0.49 mmol) in $CHCl_3$ (15 ml) was layered firstly with neat CH_2Cl_2 (15 ml) and secondly with a solution of 4,4′-bipyridine (0.08 g, 0.51 mmol) in THF (10 ml). After 12 h, mixing of all three phases was complete and a purple microcrystalline precipitate had formed, which was found to be insoluble in all common solvents at ambient temperature. Yield 0.20 g (96%). − IR (KBr, cm^{-1}): $\tilde{\nu}$ = 1622 (vs), 1540 (m), 1493 (m) (bipy-C−C, C−N), 1075 (s), 1061 (s) (B−N). − $[C_{24}H_{28}B_2FeN_2]_n$ (421.97)$_n$: calcd. C 68.31, H 6.69, N 6.64; found C 67.91, H 6.62, N 6.48.

Preparation of [**2**·pyetpy]$_n$: A solution of 1,2-bis(4-pyridyl)ethane (0.13 g, 0.71 mmol) in toluene (20 ml) was added dropwise with stirring to **2** (0.19 g, 0.71 mmol) in toluene (20 ml). The resultant orange slurry was stirred for 4 h, the insoluble material was collected on a frit (G3), triturated with hexane (5 ml), and dried in vacuo. The product was found to be insoluble in all common solvents at ambient temperature. Yield 0.25 g (78%). − IR (KBr, cm^{-1}): $\tilde{\nu}$ = 1626 (vs), 1567 (w), 1506 (m) (pyetpy-C−C, C−N), 1073 (m), 1059 (s) (B−N). − $[C_{26}H_{32}B_2FeN_2]_n$ (450.03)$_n$: calcd. C 69.39, H 7.17, N 6.22; found C 69.33, H 7.27, N 6.26.

X-ray Crystal Structure Analysis of **1**·bipy·**1**:[42] A selected purple crystal of **1**·bipy·**1** was placed in perfluorinated oil and mounted in a glass capillary on an Image Plate Diffraction System (IPDS, STOE). Final lattice parameters were obtained by least-squares refinement of 2988 reflections (graphite monochromator, λ = 0.71073 Å, Mo-K_α). Empirical formula $C_{34}H_{38}B_2Fe_2N_2$, formula weight = 608.00, triclinic system, space group $P\bar{1}$ (I.T. no.: 2); a = 8.7143(5) Å, b = 13.8257(10) Å, c = 15.8214(12) Å, α = 65.820(7), β = 86.337(7), γ = 75.376(7), V = 1680.9(2) Å^3, crystal size 0.20 × 0.13 × 0.13 mm, Z = 2, F(000) = 636. Data were collected at 293 K, distance from crystal to image plate 70 mm (10.2° < Θ < 24.7°), 300 images collected, 0° < φ < 300°, Δφ = 1°, exposure time 5 min. Data were corrected for Lorentz and polarization terms.[52] A decay and absorption correction (μ = 8.9 cm^{-1}) was performed using the program DECAY;[52] 19554 data measured, 4982 independent reflections used for refinement. The structure was solved by direct methods and refined with standard difference Fourier techniques.[53] All hydrogen atoms of **1**·bipy·**1** were calculated in ideal positions (riding model). **1**·bipy·**1** crystallizes together with 0.5 equiv. of toluene (NMR spectroscopy; elemental analysis). Severe disorder of the toluene molecules precluded their structural refinement to any satisfactory level. We have therefore applied the "squeeze" routine[54] to remedy this disordered solvent problem (potential solvent accessible area: 293 Å^3). Number of parameters refined: 361, 13.8 data per parameter, weighting scheme w = 1/$[\sigma^2(F_o^2) + (0.0176{\cdot}P)^2]$ where $P = (F_o^2 + 2{\cdot}F_c^2)/3$, shift/error < 0.001 in the last cycle of refinement, residual electron density +0.15 eÅ^{-3}, −0.18 eÅ^{-3}, $R1$ = 0.0319 [$I > 2\sigma(I)$], $wR2$ = 0.0558 (all data), the minimized function was $\Sigma w(F_o^2 - F_c^2)^2$. Neutral atom scattering factors for all atoms and anomalous dispersion corrections for the non-hydrogen atoms were taken from the *International Tables for X-ray Crystallography*.[55] All calculations were performed with a DEC 3000 AXP workstation with the STRUX-V system,[56] incorporating the programs PLATON-92,[57] PLUTON-92,[57] SHELXS-86,[58] SIR-92,[53] and SHELXL-93.[59]

Electrochemical Measurements: Cyclic voltammetry and controlled potential coulometry were performed in deaerated dimethylformamide (DMF) and CH_2Cl_2 solutions containing $[NEt_4][PF_6]$ (0.1 mol·dm^{-3}) and $[NBu_4][ClO_4]$ (0.2 mol·dm^{-3}), respectively, as supporting electrolytes. All potential values are referred to the Saturated Calomel Electrode (S.C.E.). The apparatus for electrochemistry measurements is described in ref.[60].

☆ Dedicated to Professor *Heinrich Nöth* with gratitude on the occasion of his 70th birthday.

[1] I. Manners, *Angew. Chem.* **1996**, *108*, 1712−1731; *Angew. Chem. Int. Ed. Engl.* **1996**, *35*, 1602−1621.
[2] D. W. Bruce, D. O'Hare, *Inorganic Materials*, Wiley, New York, **1992**.
[3] L. Oriol, J. L. Serrano, *Adv. Mater.* **1995**, *7*, 348−369.
[4] D. A. Foucher, B.-Z. Tang, I. Manners, *J. Am. Chem. Soc.* **1992**, *114*, 6246−6248.
[5] I. Manners, *Adv. Organomet. Chem.* **1995**, *37*, 131−168.
[6] J. B. Sheridan, K. Temple, A. J. Lough, I. Manners, *J. Chem. Soc., Dalton Trans.* **1997**, 711−713.
[7] T. L. Hennigar, D. C. MacQuarrie, P. Losier, R. D. Rogers, M. J. Zaworotko, *Angew. Chem.* **1997**, *109*, 1044−1046; *Angew. Chem. Int. Ed. Engl.* **1997**, *36*, 972−973.
[8] F. Jäkle, T. Priermeier, M. Wagner, *Chem. Ber.* **1995**, *128*, 1163−1169.
[9] F. Jäkle, K. Polborn, M. Wagner, *Chem. Ber.* **1996**, *129*, 603−606.
[10] F. Fabrizi de Biani, F. Jäkle, M. Spiegler, M. Wagner, P. Zanello, *Inorg. Chem.* **1997**, *36*, 2103−2111.
[11] E. Herdtweck, F. Peters, W. Scherer, M. Wagner, *Polyhedron* **1998**, *17*, 1149−1157.
[12] J. C. Kotz, E. W. Post, *Inorg. Chem.* **1970**, *9*, 1661−1669.

[13] W. Ruf, M. Fueller, W. Siebert, *J. Organomet. Chem.* **1974**, *64*, C45−C47.
[14] T. Renk, W. Ruf, W. Siebert, *J. Organomet. Chem.* **1976**, *120*, 1−25.
[15] W. Ruf, T. Renk, W. Siebert, *Z. Naturforsch., B* **1976**, *31b*, 1028−1034.
[16] A. Appel, H. Nöth, M. Schmidt, *Chem. Ber.* **1995**, *128*, 621−626.
[17] H. C. Brown, X. R. Mihm, *J. Am. Chem. Soc.* **1955**, *77*, 1723−1726.
[18] J. M. Essery, K. Schofield, *J. Chem. Soc.* **1961**, 3939−3953.
[19] S. Hünig, H. Berneth, *Top. Curr. Chem.* **1980**, *92*, 1−44.
[20] A. J. Bard, A. Ledwith, H. J. Shine, *Adv. Phys. Org. Chem.* **1976**, *13*, 155−278.
[21] A. J. Bard, *Nature* **1995**, *374*, 13.
[22] P. Hanson, *Adv. Heterocycl. Chem.* **1979**, *25*, 205−301.
[23] A. Factor, G. E. Heinsohn, *J. Polym. Sci. B* **1971**, *9*, 289−295.
[24] M. S. Simon, P. T. Moore, *J. Polym. Sci., Polym. Chem. Ed.* **1975**, *13*, 1−16.
[25] H. Sato, T. Tamamura, *J. Appl. Polym. Sci.* **1979**, *24*, 2075−2085.
[26] H. Kamogawa, H. Mizuno, Y. Todo, M. Nanasawa, *J. Polym. Sci.* **1979**, *17*, 3149−3157.
[27] W. Kaim, *Chem. Ber.* **1981**, *114*, 3789−3800.
[28] W. Kaim, *J. Organomet. Chem.* **1983**, *241*, 157−169.
[29] A. Lichtblau, H.-D. Hausen, W. Schwarz, W. Kaim, *Inorg. Chem.* **1993**, *32*, 73−78.
[30] J. Fiedler, S. Zalis, A. Klein, F. M. Hornung, W. Kaim, *Inorg. Chem.* **1996**, *35*, 3039−3043.
[31] F. Fabrizi de Biani, T. Gmeinwieser, E. Herdtweck, F. Jäkle, F. Laschi, M. Wagner, P. Zanello, *Organometallics* **1997**, *16*, 4776−4787.
[32] F. Peters, M. Wagner, manuscript in preparation.
[33] P. Krumholz, *J. Am. Chem. Soc.* **1951**, *73*, 3487−3492.
[34] H. Nöth, B. Wrackmeyer, *Nuclear Magnetic Resonance Spectroscopy of Boron Compounds*, in *NMR Basic Principles and Progress* (Eds.: P. Diehl, E. Fluck, R. Kosfeld), Springer Verlag, Berlin, **1978**.
[35] H. Friebolin, *Basic One- and Two-Dimensional NMR Spectroscopy*, 2nd ed., Verlag Chemie, Weinheim, **1992**.
[36] S. Hünig, I. Wehner, *Liebigs Ann. Chem.* **1989**, 299−301.
[37] H. C. Brown, R. R. Holmes, *J. Am. Chem. Soc.* **1956**, *78*, 2173−2176.
[38] K.-H. Töpel, K. Hensen, J. W. Bats, *Acta Crystallogr., C* **1984**, *40*, 828−830.
[39] N. N. Greenwood, K. Wade, *J. Chem. Soc.* **1960**, 1130−1141.
[40] H. Luther, D. Mootz, F. Radwitz, *J. Prakt. Chemie* **1957**, *5*, 242−259.
[41] A. R. Katritzky, *J. Chem. Soc.* **1959**, 2049−2051.
[42] Further details of the crystal structure investigations are available on request from the Fachinformationszentrum Karlsruhe, Gesellschaft für wissenschaftlich-technische Information mbH, D-76344 Eggenstein-Leopoldshafen (Germany), on quoting the depository number CSD-408518.
[43] F. H. Allen, O. Kennard, R. Taylor, *Acc. Chem. Res.* **1983**, *16*, 146−153.
[44] K.-H. Töpel, K. Hensen, M. Trömel, *Acta Crystallogr., B* **1981**, *37*, 969−971.
[45] E. R. Brown, J. Sandifer, in *Physical Methods in Chemistry: Electrochemical Methods* (Eds.: B. W. Rossiter, J. F. Hamilton), Wiley, New York, **1986**.
[46] A. Togni, T. Hayashi (Eds.), *Ferrocenes*, VCH Verlagsgesellschaft, Weinheim, **1995**.
[47] P. J. Haines, *Thermal Methods of Analysis, Principles, Applications and Problems*, Blackie Academic Press, London, **1995**. Note: Only a qualitative interpretation of data obtained under isochoric conditions is possible due to the limited stability of the aluminum crucibles used. At temperatures exceeding 250°C, large pressure build-up may lead to some leakage such that the reaction volume is no longer strictly constant.
[48] H.-G. Wiedemann, G. Bayer, *Top. Curr. Chem.* **1978**, *77*, 67−140.
[49] R. P. Sijbesma, F. H. Beijer, L. Brunsveld, B. J. B. Folmer, J. H. K. K. Hirschberg, R. F. M. Lange, J. K. L. Lowe, E. W. Meijer, *Science* **1997**, *278*, 1601−1604.
[50] H.-D. Hausen, A. Schulz, W. Kaim, *Chem. Ber.* **1988**, *121*, 2059−2061.
[51] J. Baumgarten, C. Bessenbacher, W. Kaim, T. Stahl, *J. Am. Chem. Soc.* **1989**, *111*, 2126−2131.
[52] IPDS Operating System Version 2.6. STOE & CIE GmbH, Darmstadt, Germany, **1995**.
[53] A. Altomare, G. Cascarano, C. Giacovazzo, A. Guagliardi, M. C. Burla, G. Polidori, M. Camalli, *SIR-92*, University of Bari, Italy, **1992**.
[54] A. Spek, *SQUEEZE, An Effective Cure for the Disordered Solvent Syndrome in Crystal Structure Refinement*, ACA-94, Atlanta, USA, **1994**, Abstract M05 (p. 66).
[55] *International Tables for Crystallography*, vol. C, tables 6. 1. 1. 4 (pp. 500−502), 4.2.6.8 (pp. 219−222) and 4.2.4.2 (pp. 193−199) (Ed.: A. J. C. Wilson), Kluwer Academic Publishers, Dordrecht, **1992**.
[56] G. Artus, W. Scherer, T. Priermeier, E. Herdtweck, *STRUX-V, A Program System to Handle X-ray Data*, TU München, Germany, **1994**.
[57] A. L. Spek, *Acta Crystallogr., A* **1990**, *46*, C34.
[58] G. M. Sheldrick, *SHELXS-86: Program for Crystal Structure Solutions*, Universität Göttingen, Germany, **1986**.
[59] G. M. Sheldrick, "SHELXL-93" in *Crystallographic Computing 3* (Eds.: G. M. Sheldrick, C. Krüger, R. Goddard), Oxford University Press, **1993**.
[60] C. Bianchini, F. Laschi, D. Masi, F. M. Ottaviani, A. Pastor, M. Peruzzini, P. Zanello, F. Zanobini, *J. Am. Chem. Soc.* **1993**, *115*, 2723−2730.

[98092]